A General T-Stub Circuit for Decoupling of Two Dual-Band Antennas

Jiangwei Sui and Ke-Li Wu, *Fellow, IEEE*

***Abstract*— This paper presents a novel technique for decoupling of two closely spaced dual-band antennas using T-stub circuits. A decoupling circuit consists of three T-stub elements, each of which provides the required phases and impedances in dual frequency bands independently. A set of general design formulas is derived for determining the electric parameters of required T-stubs. To validate the new decoupling technique, a pair of dual-band inverted-F antennas working in the 2.45- and 5.8-GHz bands and another pair of dual-band monopole antennas working in the 2.4- and 5.2-GHz bands with and without the decoupling circuit are designed, prototyped, and measured. The measured S-parameters correlate with the theoretical designed data very well. With the decoupling circuit, significant improvement in antenna efficiency and data throughput demonstrates that the technique is useful for wireless terminals, where dual-band multiple-input and multiple-output antennas are used.**

***Index Terms*— Decoupling circuit, dual-band, impedance transformer, multiple-input and multiple-output (MIMO), quarter-wavelength transmission line, single-channel full duplex, T-stub.**

I. Introduction

MULTI-BAND and multimode wireless terminals have become a mainstream technology today to accommodate the demands for heterogeneous wireless communication systems including not only multiple band 3G and 4G systems but also multiple band WLAN systems. To improve the data throughput in a multipath environment, the multiple input and multiple output (MIMO) technology using multiple antennas has been becoming more and more popular nowadays, from 4G smart phones to Wi-Fi modules. However, due to the compact volume of a mobile terminal, in which the distance between antennas is usually small in terms of wavelength, strong electromagnetic coupling among the multiple antennas severely diminishes the benefit brought by the MIMO system [1], [2]. Moreover, full duplex communication scheme has a large potential to be adopted in 5G systems to increase the spectral efficiency [3], for which a high isolation between the transmitting and receiving antenna ports would be crucial for achieving good full duplex quality.

Manuscript received October 24, 2016; accepted December 24, 2016. Date of publication January 26, 2017; date of current version June 2, 2017. This work was supported in part by The Chinese University of Hong Kong through a post-graduate scholarship and in part by the Development and Reform Commission of Shenzhen Municipality under Grant Shen Fa Gai (2013) 1673.

The authors are with the Department of Electronic Engineering, The Chinese University of Hong Kong, Hong Kong, and also with the Shenzhen Engineering Laboratory of Wireless Locating Technology and System, Shenzhen Research Institute, The Chinese University of Hong Kong, 518000 Shenzhen, Hong Kong (e-mail: jwsui@ee.cuhk.edu.hk; klwu@ee.cuhk.edu.hk).

Color versions of one or more of the figures in this paper are available online at http://ieeexplore.ieee.org.

Digital Object Identifier 10.1109/TMTT.2017.2647951

In the past few decades, many decoupling techniques have been proposed to reduce the unwanted coupling between two antennas [4]–[11]. Although these techniques achieve good isolation at the antenna ports, they mostly pay attention to decoupling between two single band antennas. Until recently, the problem of reducing mutual couplings of two dual-band antennas has gained much attention in the community. There are mainly two categories of antenna decoupling techniques: antenna dependent [12]–[16] and antenna independent [17]–[20]. Two dual-element dual-band antenna systems for mobile terminals using defected ground structure technique are proposed in [12] and [13]. A dual-band MIMO antenna system is designed with an isolation stub structure inserted between the two antennas for reducing the coupling of two antennas in [14]. A compact dual-band LTE antenna system is designed using a neutralization line structure to reduce the coupling of the two bands in [15]. An SIW cavity antenna MIMO system is designed using polarization diversity and shorted edges in [16]. The above-mentioned works are referred to as decoupled antennas design because the decoupling element is a part of antennas and must be designed altogether with the antenna structure. Although the schemes in this category can help to improve the isolation between the two antennas, they are all antenna dependent and require a good sense to design for a specific antenna configuration.

The second decoupling category is antenna independent. This category is based on the S-parameters of two coupled antennas so that it can be generally used for any specific antenna configuration. In this direction, a set of lumped element dual-band decoupling and matching networks for a pair of dual-band antennas are proposed in [17]. By employing LC circuits to realize decoupling network, dual-band matching network at each antenna port is inevitable, which may seriously limit the impedance matching bandwidth. In addition, the unavoidable parasitic effect of the lumped elements makes it unsuitable for higher frequency applications, for example 5 GHz band adopted in IEEE 802.11ac. A dual-band rat-race coupler is used to reduce the coupling of two dual-band MIMO antennas in [18]. The scheme provides good pattern diversity and improvement of the antenna port isolation using a mode-decoupling network. A decoupling network using synthesized microstrip line is also proposed in [19]. The reactive decoupling technique is used for the upper band and the eigenmode feed network is cascaded to the shunt connected reactive element for reducing the mutual coupling at the lower band. However, two separate decoupling circuits for high and low bands successively enlarge the size and design complexity of the dual-band decoupling network.

Very recently, a circuit scheme of two shunt connected coupled resonator network is proposed for two dual-band coupled antennas using the first two resonant modes in two coupled resonators [20]. Although the dimensions of the resonators can be tuned to achieve good decoupling effect in dual bands, the decoupling network significantly deteriorates the original matching condition in the dual bands, which is common in existing dual-band decoupling techniques in this category. In all these approaches, additional dedicated matching networks at each antenna port that are well matched naturally by the antennas themselves are required.

T-stub circuit has found many applications in designing dual-band microwave devices that employ quarter-wavelength transmission line property at two frequencies. An open-circuit T-stub circuit is used as a dual-band quarter-wavelength transmission line in a dual-band coupler [21]. A dual-band Doherty power amplifier is proposed using a T-stub circuit serving as a dual-band quarter-wavelength transmission line in [22]. The T-stub circuit is utilized in two places in a dual-band Doherty power amplifier [23], one for a dual-band quarter-wavelength transmission line and another for a dual-band delay line with 180° phase difference at the two frequencies.

In this paper, a generic RF circuit for decoupling two dual-band antennas is proposed using a generalized T-stub circuit that provides arbitrary phase shift and arbitrary impedance values at two frequencies independently. The decoupling circuit consists of three generalized T-stubs, each of which serves as a dual-band transmission line with specific phase and impedance values independently. Comparing to the existing dual-band decoupling techniques, the proposed dual-band decoupling network has the following unique features.

1) The circuit can not only satisfy decoupling but also matching conditions in two designated frequency bands, no extra matching circuits are needed.
2) The circuit is antenna independent and can be designed to accommodate different coupling levels in two bands, independently.
3) The design process is deterministic and the design formula is well developed in this paper.

This paper is organized as follows. The working principle and the design theory of the proposed decoupling circuit are presented in Section II followed by two proof-of-concept design examples in Section III. Finally, conclusions are given in Section IV.

II. Working Principle and Design Theory

A. Proposed Decoupling Circuitry

Fig. 1 shows the proposed dual-band decoupling circuitry inserted between two coupled dual-band antennas, among which the coupling levels and coupling mechanisms (either capacitive or inductive) in each working band are different. Among all the cases being investigated, the coupling signs in the low band and the high band are found to be always opposite, which coincides with the finding in [20]. It is understandable that for most cases the lower the frequency the stronger the coupling is, due to the shorter electrical length for the same physical distance. At each antenna port, a two-port short-circuit T-stub (SC-T-S) is serially connected for independently controlling the phase shifting in each band. Another SC-T-S is shunt connected between the two ports to be decoupled. The shunt connected SC-T-S plays the role of a dual-band neutralization-line, whose characteristics in each frequency band can be independently controlled. It is anticipated that the two coupled antennas are well matched before applying the decoupling circuitry.

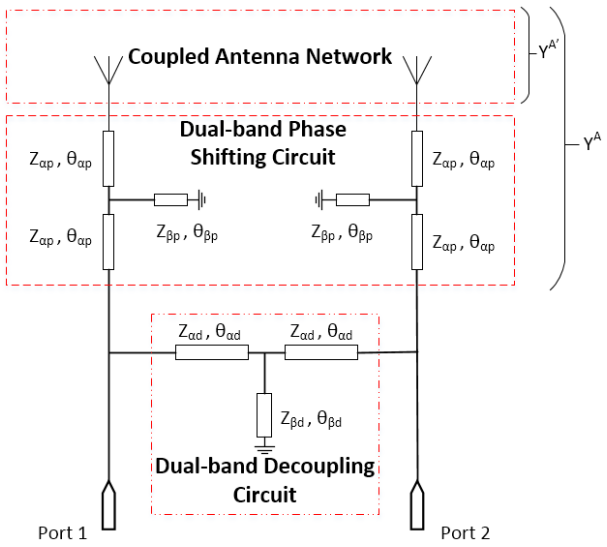

Fig. 1. Circuit schematic of the proposed dual-band decoupling circuit.

In this paper, the T-stub is equivalent to a dual-band transmission line with arbitrary electrical length and arbitrary characteristic impedance in the two frequencies. It will be shown that the T-stub circuits used in [21]–[23] are special cases of the equivalence. The details are given in Section II-C.

B. Decoupling and Matching Conditions

It is assumed that two coupled antennas with and without serially connected T-stub circuits are represented by 2-by-2 admittance matrices $[Y^A]$ and $[Y^{A'}]$, respectively, where $[Y^{A'}]$ is defined at the original ports and is with complex entries, and the admittance matrix of the shunt connected T-stub circuit is denoted by $[Y^D]$. Obviously, the total admittance of the antenna pairs with two serially connected T-stubs and the shunt connected T-stub is the sum of the two individual admittance matrices as

$$\begin{bmatrix} Y_{11}(f) & Y_{12}(f) \\ Y_{21}(f) & Y_{22}(f) \end{bmatrix} = \begin{bmatrix} Y_{11}^A(f) + Y_{11}^D(f) & Y_{12}^A(f) + Y_{12}^D(f) \\ Y_{21}^A(f) + Y_{21}^D(f) & Y_{22}^A(f) + Y_{22}^D(f) \end{bmatrix} \tag{1}$$

where f is the bandpass frequency.

Note that the entries of $[Y^D]$ are purely imaginary. Then the decoupling conditions in the center frequencies of the desired two frequency bands can be expressed as

$$\mathrm{Re}\{Y_{21}^A(f_L)\} \approx 0 \tag{2a}$$

$$\mathrm{Im}\{Y_{21}^A(f_L)\} + Y_{21}^D(f_L) \approx 0 \tag{2b}$$

$$\mathrm{Re}\{Y_{21}^A(f_H)\} \approx 0 \tag{3a}$$

$$\mathrm{Im}\{Y_{21}^A(f_H)\} + Y_{21}^D(f_H) \approx 0 \tag{3b}$$

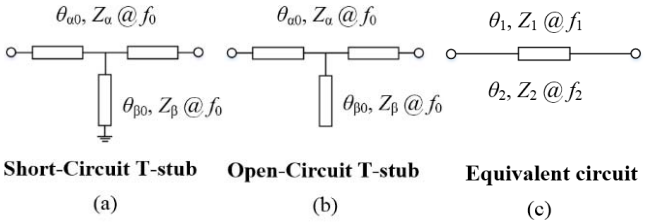

Fig. 2. T-stub circuits and their equivalent circuit. (a) Short-circuit T-stub. (b) Open-circuit T-stub. (c) Equivalent circuit.

and the matching conditions are

$$j \cdot \mathrm{Im}\{Y_{kk}^A(f_L)\} + Y_{kk}^D(f_L) \approx 0, \quad k = 1, 2 \tag{4a}$$

$$j \cdot \mathrm{Im}\{Y_{kk}^A(f_H)\} + Y_{kk}^D(f_H) \approx 0, \quad k = 1, 2 \tag{4b}$$

where f_L and f_H denote the center frequencies of the low and high frequency bands, respectively.

The above conditions imply that: 1) the two serially connected T-stubs should be matched to the antenna ports with appropriate phase shift so that the real part of Y_{21}^A becomes zero at both f_L and f_H; 2) the mutual admittance of the shunt connected T-stub cancels out that of Y_{21}^A; and 3) its self-admittance of the shunt connected T-stub cancels out that of Y_{11}^A.

C. Analysis of T-Stub Dual-Band Circuits

Fig. 2 shows two T-stub circuits, namely, SC-T-S circuit and open-circuit T-stub circuit, as well as their dual-band equivalent circuit. Denote f_1 and f_2 as the center frequencies of the low and the high bands, respectively, and set

$$f_0 = \frac{f_1 + f_2}{2}. \tag{5}$$

Without losing generality, only the analysis of the SC-T-S circuit as shown in Fig. 2(a) is given. The ABCD coefficients of the T-stub circuit can be found as (6), shown at the bottom of this page, where θ_α, Z_α, θ_β and Z_β are the electrical length and characteristic impedance of the series arms and the shunt stub at frequency f. Thus

$$\theta_\alpha = \theta_{\alpha 0}\frac{f}{f_0}, \quad \theta_\beta = \theta_{\beta 0}\frac{f}{f_0}. \tag{7}$$

Comparing the entries of the ABCD matrix with their corresponding entries of the equivalent circuit shown in Fig. 2(c), the following four equations can be obtained:

$$\cos\left(2\theta_{\alpha 0}\frac{f_1}{f_0}\right) + \frac{1}{2}\frac{Z_\alpha}{Z_\beta}\sin\left(2\theta_{\alpha 0}\frac{f_1}{f_0}\right)\cot\left(\theta_{\beta 0}\frac{f_1}{f_0}\right) = \cos\theta_1 \tag{8}$$

$$\cos\left(2\theta_{\alpha 0}\frac{f_2}{f_0}\right) + \frac{1}{2}\frac{Z_\alpha}{Z_\beta}\sin\left(2\theta_{\alpha 0}\frac{f_2}{f_0}\right)\cot\left(\theta_{\beta 0}\frac{f_2}{f_0}\right) = \cos\theta_2 \tag{9}$$

$$Z_\alpha \sin\left(2\theta_{\alpha 0}\frac{f_1}{f_0}\right) + \frac{Z_\alpha^2}{Z_\beta}\sin^2\left(\theta_{\alpha 0}\frac{f_1}{f_0}\right)\cot\left(\theta_{\beta 0}\frac{f_1}{f_0}\right) = Z_1\sin\theta_1 \tag{10}$$

$$Z_\alpha \sin\left(2\theta_{\alpha 0}\frac{f_2}{f_0}\right) + \frac{Z_\alpha^2}{Z_\beta}\sin^2\left(\theta_{\alpha 0}\frac{f_2}{f_0}\right)\cot\left(\theta_{\beta 0}\frac{f_2}{f_0}\right) = Z_2\sin\theta_2. \tag{11}$$

Note that (Z_1, θ_1) at f_1, and (Z_2, θ_2) at f_2 are prespecified parameters. From (8) and (10), the following relation can be obtained:

$$\tan\left(\theta_{\alpha 0}\frac{f_1}{f_0}\right) = \frac{Z_1}{Z_\alpha}\tan\left(\frac{\theta_1}{2}\right). \tag{12}$$

Similarly, the following relation can be obtained from (9) and (11):

$$\tan\left(\theta_{\alpha 0}\frac{f_2}{f_0}\right) = \frac{Z_2}{Z_\alpha}\tan\left(\frac{\theta_2}{2}\right). \tag{13}$$

Accordingly, coefficient $\theta_{\alpha 0}$ can be easily obtained by solving

$$\frac{\tan\left(\theta_{\alpha 0}\frac{f_1}{f_0}\right)}{\tan\left(\theta_{\alpha 0}\frac{f_2}{f_0}\right)} = \frac{Z_1}{Z_2}\frac{\tan\left(\frac{\theta_1}{2}\right)}{\tan\left(\frac{\theta_2}{2}\right)}. \tag{14}$$

Note that the left-hand side of (14) is a single variable function of $\theta_{\alpha 0}$, and the right-hand side is a constant. This equation can be solved by either numerical or graphical method easily.

Having known $\theta_{\alpha 0}$, Z_α can be obtained according to (12) or (13). Similarly with $\theta_{\alpha 0}$, $\theta_{\beta 0}$ can be found from the following equation:

$$\frac{\cot\left(\theta_{\beta 0}\frac{f_1}{f_0}\right)}{\cot\left(\theta_{\beta 0}\frac{f_2}{f_0}\right)} = \frac{\cos\theta_1 - \cos\left(2\theta_{\alpha 0}\frac{f_1}{f_0}\right)}{\sin\left(2\theta_{\alpha 0}\frac{f_1}{f_0}\right)}\frac{\sin\left(2\theta_{\alpha 0}\frac{f_2}{f_0}\right)}{\cos\theta_2 - \cos\left(2\theta_{\alpha 0}\frac{f_2}{f_0}\right)}. \tag{15}$$

which is derived from (8) and (9). Consequently, Z_β can be obtained by (8) or (9). At this point, all the parameters, $\theta_{\alpha 0}$, Z_α, $\theta_{\beta 0}$, and Z_β of an SC-T-S are obtained for any prescribed Z_1, θ_1, Z_2, and θ_2. By the same token, the design equations for open-circuit T-stub circuit can also be derived. For the purpose

$$\begin{bmatrix} A & jB \\ jC & D \end{bmatrix} = \begin{bmatrix} \cos(2\theta_\alpha) + \frac{1}{2}\frac{Z_\alpha}{Z_\beta}\sin(2\theta_\alpha)\cot\theta_\beta & j\left(Z_\alpha\sin(2\theta_\alpha) + \frac{Z_\alpha^2}{Z_\beta}\sin^2\theta_\alpha\cot\theta_\beta\right) \\ j\left(\frac{1}{Z_\alpha}\sin(2\theta_\alpha) - \frac{1}{Z_\beta}\cos^2\theta_\alpha\cot\theta_\beta\right) & \cos(2\theta_\alpha) + \frac{1}{2}\frac{Z_\alpha}{Z_\beta}\sin(2\theta_\alpha)\cot\theta_\beta \end{bmatrix} \tag{6}$$

of brevity, only the results are listed here as

$$\tan\left(\theta_{\alpha 0}\frac{f_1}{f_0}\right) = \frac{Z_1}{Z_\alpha}\cot\left(\frac{\theta_1}{2}\right) \tag{16a}$$

$$\tan\left(\theta_{\alpha 0}\frac{f_2}{f_0}\right) = \frac{Z_2}{Z_\alpha}\cot\left(\frac{\theta_2}{2}\right) \tag{16b}$$

$$Z_\alpha \tan\left(\theta_{\beta 0}\frac{f_1}{f_0}\right) = 2Z_\beta \frac{\cos\left(2\theta_{\alpha 0}\frac{f_1}{f_0}\right) - \cos\theta_1}{\sin\left(2\theta_{\alpha 0}\frac{f_1}{f_0}\right)} \tag{16c}$$

$$Z_\alpha \tan\left(\theta_{\beta 0}\frac{f_2}{f_0}\right) = 2Z_\beta \frac{\cos\left(2\theta_{\alpha 0}\frac{f_2}{f_0}\right) - \cos\theta_2}{\sin\left(2\theta_{\alpha 0}\frac{f_2}{f_0}\right)}. \tag{16d}$$

D. Serial T-stub Circuit for Dual-Band Phase Shifting

In general, the real part of the mutual admittance of $[Y^{A\prime}]$ is nonzero. To satisfy (2a) and (3a), the admittance needs to be transformed to a pure imaginary value by adding, at each antenna port, an appropriate phase shifting circuit. The circuit realizes designated phase advancement θ_1 and θ_2 in the low and high frequencies, respectively, while maintaining antenna's matching condition. In this paper, the SC-T-S is adopted for this purpose.

Assume $Z_1 = Z_2 = 50\ \Omega$ in Fig. 2(c). Based on the desired θ_1 and θ_2 at f_1 and f_2, respectively, the parameters $\theta_{\alpha 0}$, Z_α, $\theta_{\beta 0}$ and Z_β can be obtained according to the formulas derived in Section II-C. To give an idea for a possible solution region, two practical cases are studied. For case 1, $f_1 = 2.45$ GHz and $f_2 = 5.8$ GHz; and for case 2, $f_1 = 2.45$ GHz and $f_2 = 5.25$ GHz. Considering the realization constrains, $\theta_{\alpha 0}$ and $\theta_{\beta 0}$ are limited in the range of [0°, 120°] and Z_α and Z_β are limited in the range of [25 Ω, 150 Ω]. Besides, the return loss of better than −25 dB is set as the good matching condition. Under these conditions, the solution regions can be obtained from the design equations for the two cases. The shaded area in Fig. 3(a) shows the solution region for case 1 and the region bounded by a dashed line is for case 2.

As shown in Fig. 3(a), when $\theta_1 \in [50°, 115°]$, the corresponding θ_2 can have more than 50° adjustable range. This is attractive for many practical dual-band applications. For the θ_1 that is not in the solution region, a short section of transmission line can be added before the phase shifting circuit to offset the desired electrical length.

It is worth mentioning that a similar solution region can be obtained for other specified f_1 and f_2 pairs. Fig. 3(b) shows the solution regions of the two cases using an open-circuit T-stub. Although the solution region for an open-circuit T-stub is narrower than that of an SC-T-S, one may find its use for small θ_1 cases.

An example for $\theta_1 = 61°$, $\theta_2 = 176°$, $Z_1 = 50\ \Omega$ and $Z_2 = 50\ \Omega$ is shown in Fig. 4 and the corresponding T-stub parameters are $\theta_{\alpha 0} = 62.9°$, $Z_\alpha = 38.6\ \Omega$, $\theta_{\beta 0} = 59.2°$, $Z_\beta = 120\ \Omega$. It is shown that the T-stub provides two desired phases and 50 Ω characteristic impedance at the two designated frequencies.

E. Shunt T-Stub Circuit for Dual-Band Decoupling

For a pair of dual-band antennas, the mutual admittance of the antennas usually presents different signs: negative in the low band and positive in the high band; or positive in the low band and negative in the high band. One can always make the coupling negative in the low band and positive in the high band by shifting the phase at antenna ports. In this way, an SC-T-S can be used to counteract the imaginary part of Y_{21}^A as it introduces a positive imaginary part of Y_{21}^D in the low band and a negative imaginary part in the high band. According to (4a) and (4b), the T-stub also ensures a small value if nonzero of Y_{11}^D and Y_{22}^D in the low and high bands to compensate the imperfect matching condition of the coupled antennas.

For simplicity, let $Y_{11}^D = 0$ and $Y_{22}^D = 0$ here for demonstration. To ensure the self-admittance Y_{11}^D and Y_{22}^D equal

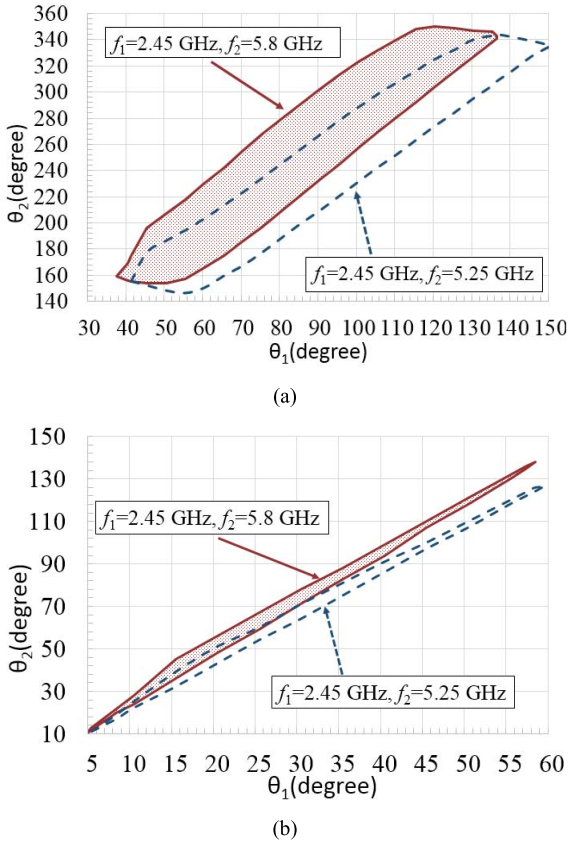

Fig. 3. Solution regions for 50-Ω phase shifting T-stub. Case 1: $f_1 = 2.45$ GHz, $f_2 = 5.8$ GHz; and case 2: $f_1 = 2.45$ GHz, $f_2 = 5.25$ GHz, where $\theta_{\alpha 0}$ and $\theta_{\beta 0}$ are confined in [0°, 120°], and Z_α and Z_β are confined in [25 Ω, 150 Ω]. (a) Short-circuit T-Stub. (b) Open-circuit T-stub.

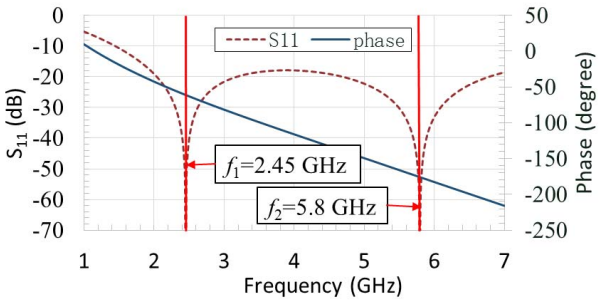

Fig. 4. Simulated return loss and transmission phase of a phase-shifting T-stub, $f_1 = 2.45$ GHz, $f_2 = 5.8$ GHz for $\theta_1 = 61°$, $\theta_2 = 176°$, $Z_1 = 50\ \Omega$, and $Z_2 = 50\ \Omega$.

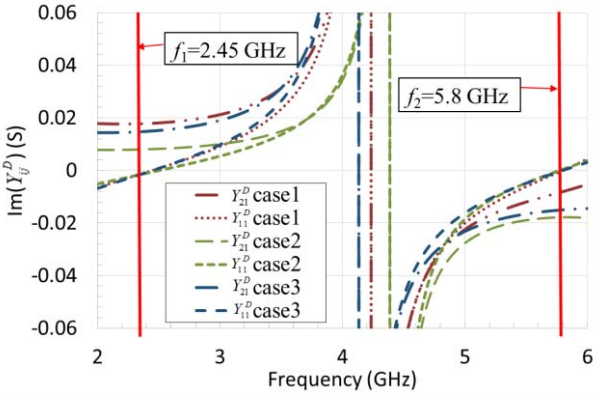

Fig. 5. Simulated admittance of the shunt T-stub for three cases.

TABLE I
SOLUTIONS OF DECOUPLING CIRCUIT FOR THREE TYPICAL CASES

	Y_{21l}^D (S)	Y_{21h}^D (S)	$\theta_{\alpha 0}$(°)	Z_α(Ω)	$\theta_{\beta 0}$(°)	Z_β(Ω)
Case 1	0.018	-0.008	79.8	51.1	118.7	107.9
Case 2	0.008	-0.018	100.4	67.9	38.9	126.5
Case 3	0.015	-0.015	90	49.4	90	60.2

to zero and $Y_{21}^D = -Y_{21}^A$ at f_1 and f_2 and to obtain the parameters $\theta_{\alpha 0}$, Z_α, $\theta_{\beta 0}$ and Z_β, one can set $\theta_1 = 90°$, $\theta_2 = 270°$, $Z_1 = -1/Y_{21l}^A$ and $Z_2 = 1/Y_{21h}^A$ in (8)–(11), where $Y_{21}^{A_l}$ and $Y_{21}^{A_h}$ represent the mutual admittance of the coupled antennas in the low and high bands, respectively.

To illustrate the applicability range, three cases representing different mutual admittance levels at 2.45 GHz (low band) and 5.8 GHz (high band) are shown in Fig. 5. The admittance values and the solutions of $\theta_{\alpha 0}$, Z_α, $\theta_{\beta 0}$ and Z_β for corresponding T-stubs are listed in Table I, where $Y_{21}^{D_l}$ and $Y_{21}^{D_h}$ represent the mutual admittance of the shunt T-stub in the low and high bands, respectively. It can be observed from Fig. 5 that the designed T-stubs provide the required mutual admittance Y_{21} at both the low and high frequencies, while the self-admittance Y_{11} of each case passes zero line in both the low and high frequencies. Of course, for cases with nonzero Y_{11}^D, the similar results can be obtained.

It is understandable that the required Y_{21}^D is determined by Y_{21}^A of the coupled antennas, which is proportional to S_{21} if antennas are reasonably well matched. Roughly speaking, 0.007 S of Y_{21}^D corresponds to about -15 dB of S_{21} and 0.015 S of Y_{21}^D corresponds to about -8 dB of S_{21}. Therefore, the range of realizable admittance value is sufficiently wide for most practical antenna coupling cases.

The same as many other dual-band microwave applications using combined transmission line, this decoupling method has an application frequency ratio range. As shown in Fig. 6, for the given three mutual admittance at low frequency $Y_{21}^{D_l}$, the mutual admittance at high frequency $Y_{21}^{D_h}$ has a large decoupling region at the frequency ratio range [2, 2.5]. This range includes numerous commercial dual-band communication standards, such as GSM 900/1900, UMTS 850/2100, WIFI 2.45/5.2, and WIFI 2.45/5.8.

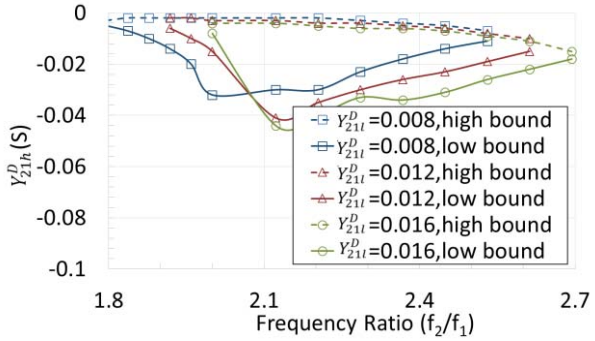

Fig. 6. Simulated decoupling region for different frequency ratios.

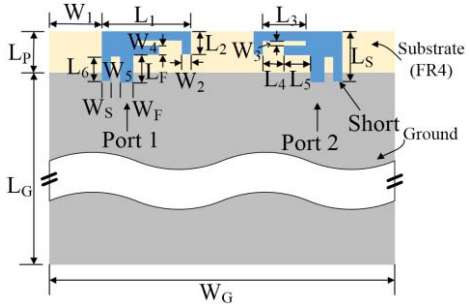

(a)

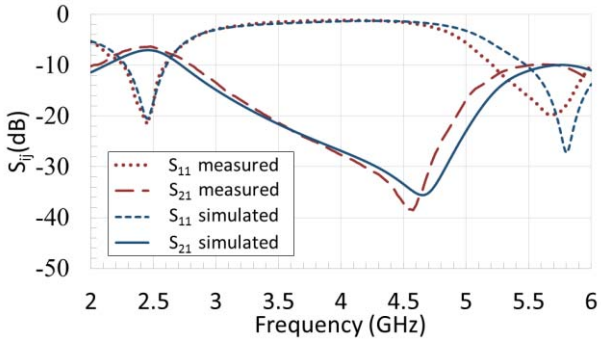

(b)

Fig. 7. (a) Layout of two dual-band coupled inverted-F antennas. (b) Simulated and measured S-parameters of the coupled antennas.

III. DESIGN EXAMPLES

To demonstrate the effectiveness of dual-band decoupling technique using T-stub circuits, two pairs of dual-band antennas are designed, simulated, and tested. In the first example, a pair of dual-band inverted-F antennas are designed on FR4 PCB circuit board with thickness of 1.6 mm and dielectric constant of 4.3. The center frequencies for the low and high bands are 2.45 and 5.8 GHz, respectively. In the second example, a pair of dual-band monopole antennas are designed on Rogers 4003C PCB circuit board with thickness of 0.81 mm and dielectric constant of 3.55. The center frequencies for the low and high bands are 2.4 and 5.2 GHz, respectively.

A. Two Dual-Band PIFAs

The layout of the coupled antennas is shown in Fig. 7(a) and the corresponding dimensions are given in Table II.

TABLE II
DIMENSIONS OF COUPLED AND DECOUPLED ANTENNAS (mm)

L_1	21.2	L_7	43.86	L_{13}	13.3	W_2	2	W_8	5.33
L_2	5.3	L_8	13.25	L_S	11.98	W_3	1.5	W_9	2
L_3	10.73	L_9	6.98	L_F	7	W_4	2	W_{10}	3.37
L_4	5.27	L_{10}	5.85	L_P	10	W_5	2.43	W_F	3.14
L_5	6.38	L_{11}	10.04	L_G	110	W_6	2	W_S	2
L_6	5.98	L_{12}	13.3	W_1	13	W_7	3.14	W_G	85

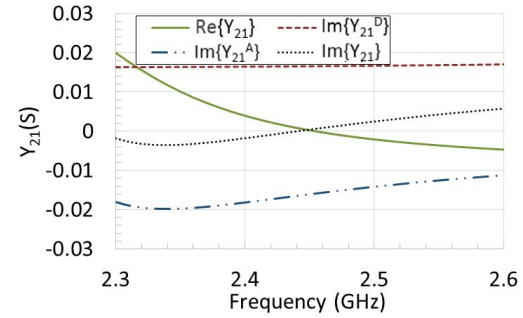

(a)

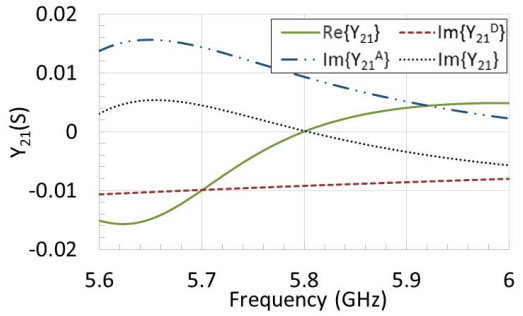

(b)

Fig. 8. Simulated total Y_{21} and imaginary part of Y_{21}^A and Y_{21}^D (a) in 2.45 GHz band and (b) 5.8 GHz band.

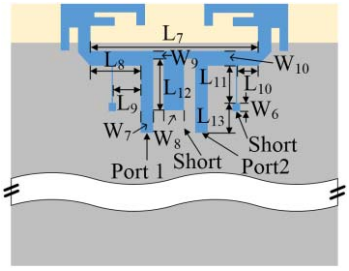

(a)

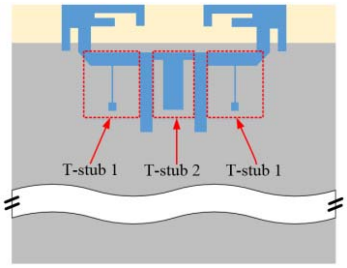

(b)

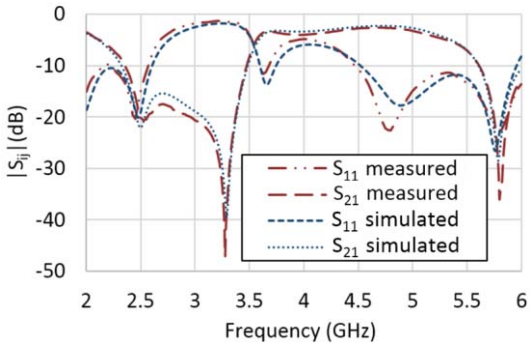

(c)

Fig. 9. (a) Dimensions of two dual-band decoupled inverted-F antennas. (b) Layout of three T-stubs. (c) Simulated and measured S-parameters of the dual-band decoupled antennas.

The edge-to-edge distance between the two antennas is 17 mm with the electrical length less than 0.14 wavelength for 2.45 GHz in free space. As shown in Fig. 7(b), the simulated and measured S-parameters agree well and the coupling between the two antennas is strong due to the short electrical distance with about -7 dB at 2.45 GHz and -10 dB at 5.8 GHz.

The SC-T-S that is serially connected to each antenna port for shifting the phase of mutual admittance parameter of $[Y^{A\prime}]$ is first designed to satisfy (2a) and (3a). It is found that with $\theta_1 = 61°$, $\theta_2 = 176°$, $Z_1 = 50\ \Omega$ and $Z_2 = 50\ \Omega$, the real part of the mutual admittance at the two frequencies is transformed to zero. According to the analysis in Sections II-C and II-D, the corresponding parameters of the T-stub for phase shifting can be obtained easily with $\theta_{\alpha 0} = 62.9°$, $Z_\alpha = 38.6\ \Omega$, $\theta_{\beta 0} = 59.2°$, and $Z_\beta = 120\ \Omega$.

With the real part of the mutual admittance of the coupled antennas being shifted to zero, the shunt connected T-stub circuit needs to be designed to cancel the mutual admittance Y_{21}^A in the dual working bands. As shown in Fig. 8, $Y_{21l}^A = -0.017$ S and $Y_{11l}^A = 0.004$S at 2.45 GHz and $Y_{21h}^A = 0.009$ S and $Y_{11h}^A = -0.004$ at 5.8 GHz. According to the design procedure given in Session II-E, the corresponding circuit parameters can be obtained as $\theta_{\alpha 0} = 79.19°$, $Z_\alpha = 44.15\ \Omega$, $\theta_{\beta 0} = 103.78°$, and $Z_\beta = 32.7\ \Omega$. It can be observed from Fig. 8 that having shunt connected the decoupling T-stub, the real part and the imaginary part of the total Y_{21} both become zero at the two frequencies. One thing should be mentioned is that since the variation of total admittance Y_{21} is very little in the two bands, the decoupling circuit can achieve a relatively wide band decoupling in both frequency bands of interest.

The layout of decoupled antennas together with two serially connected phase shifting T-stubs and a shunt connected decoupling T-stub is shown in Fig. 9(a). The three dotted rectangular boxes shown in Fig. 9(b) denote the decoupling circuit: two T-stub 1 denote the phase shifting part while T-stub 2 denotes the decoupling part. The dimensions of the circuit layout are also listed in Table II. Due to the fringe effect and the coupling effect of the microstrip line, a fine-tuning and optimization process is conducted by EM simulation. As shown in Fig. 9(c), the measured S-parameters agree well

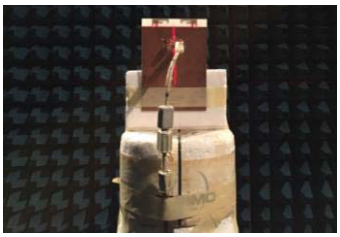

Fig. 10. Measurement setup for antenna radiation pattern and total efficiency.

with the simulated results. The isolation between the two antennas is improved from about 7 to 15 dB in the low band (2.4 to 2.5 GHz) and 10 to 20 dB in the high band (5.75 to 5.85 GHz) while the return losses of the decoupled antennas maintain about the same level as those of the coupled antennas in the two bands.

The radiation performance of the coupled antenna pair and decoupled pair are also measured using the in-house SATIMO SG128 spherical near-field scanner in an ISO17025 accredited laboratory. The measurement setup is shown in Fig. 10. The measured radiation power patterns for the coupled and decoupled antenna pairs in both the low and high frequencies are shown Fig. 11. It can be seen that the radiation patterns in both *xoz* and *yoz* planes before and after decoupling are nearly the same but the signal level for decoupled antennas is obviously higher than that of the coupled antennas, showing the improvement of the total efficiency.

The measured total efficiencies for both the low and high bands are compared in Fig. 12. It shows that in the low band, the efficiency is improved from about 60%–75% by employing the decoupling circuit while in the high band, the efficiency is improved not as much as that in low frequency band mainly due to two reasons: 1) the coupling S_{21} in high frequency band is lower than that in low frequency band so that the efficiency improvement range is lower than that in low frequency band and 2) the decoupling structure will introduce more loss using FR4 substrate for high frequency band than that in low frequency band.

To study the performance for MIMO applications, the data throughput for the coupled and decoupled antenna pairs is simulated with different signal-to-noise ratios (SNRs) using WINNER II channel model in Agilent W1715 MIMO Channel Builder in System Vue [24]. WINNER II channel model is a geometry-based model with three scenario categories: local, metropolitan, and wide areas. The scenario B1 (Urban microcell) is adopted in the comparison study. WINNER II channel models can be used in link level and system level for wireless system working in 2–6 GHz frequency range. In the simulation process, the measured 3-D complex vector antenna patterns are imported to imitate a real MIMO receiving antennas system. Two omnidirectional antennas are used as transmitting antennas in the simulation. The two coupled and decoupled antenna pairs are placed in the broadside direction of the transmitting antennas as the receiving antennas of the system. Four rotations of the receiving antennas ($\varphi = 0°$, $\varphi = 90°$, $\varphi = 180°$, and $\varphi = 270°$) are adopted in the simulation to get an averaged throughput. As shown in Fig. 13, the averaged throughput of the simulated MIMO system with

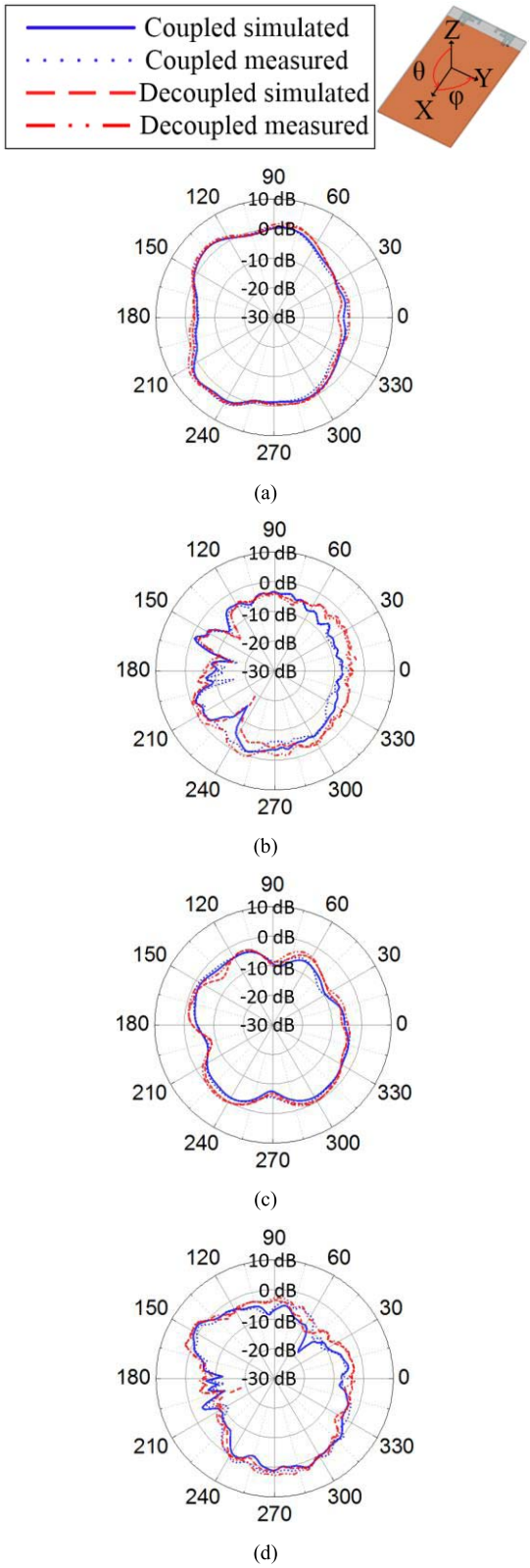

Fig. 11. Total radiation patterns of the coupled and decoupled inverted-F antennas at (a) 2.45 GHz in the *xoz* plane, (b) 5.8 GHz in the *xoz* plane, (c) 2.45 GHz in the *yoz* plane, and (d) 5.8 GHz in the *yoz* plane. Antenna 1 is excited while antenna 2 is terminated with a matched load.

decoupled antenna pairs has a significant improvement in both 2.45 and 5.8 GHz bands compared with its counterpart with coupled antennas.

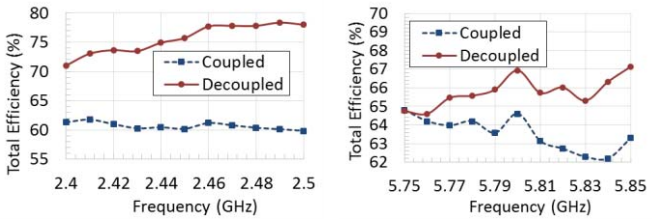

Fig. 12. Measured total efficiency for coupled and decoupled inverted-F antennas (a) in 2.45 GHz band and (b) 5.8 GHz band.

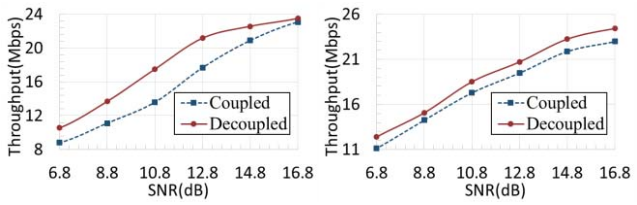

Fig. 13. Averaged throughput versus SNR for coupled and decoupled inverted-F antennas simulated in WINNER II channel model B1 (a) in 2.45 GHz band and (b) 5.8 GHz band.

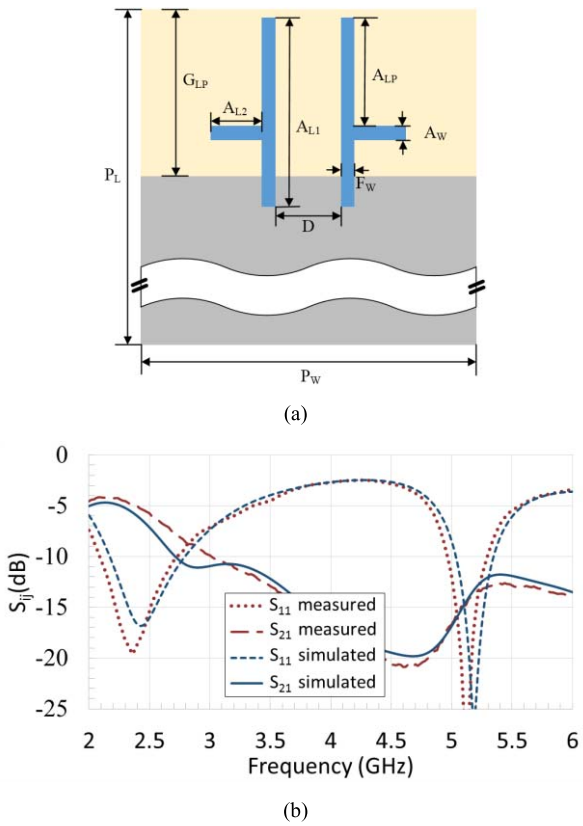

Fig. 14. (a) Layout of two dual-band coupled monopole antennas. (b) Simulated and measured S-parameters of the coupled antennas.

B. Two Dual-Band Monopole Antennas

The layout of two coupled dual-band monopole antennas is shown in Fig. 14(a) and the corresponding dimensions are given in Table III. The edge-to-edge distance between the two antennas is 10 mm with the electrical length 0.08 wavelength for 2.4 GHz in free space. As shown in Fig. 14(b), the simulated and measured S-parameters agree well and the coupling between the two antennas is strong due to the short electrical distance with about −5 dB at 2.4 GHz and −13.5 dB at 5.2 GHz.

TABLE III
DIMENSIONS OF COUPLED AND DECOUPLED ANTENNAS (mm)

P_L	90	A_{L2}	7.6	D_{W1}	3.4	D_{W3}	2.5
P_W	50	A_W	2	D_{L2}	10.2	D_{L4}	15.86
G_{LP}	25	F_W	1.8	D_{W2}	0.26	D_{W4}	3.37
A_{LP}	16	D	10	D_{L31}	2.56	F_{W1}	1.8
A_{L1}	28	D_{L1}	18.58	D_{L32}	2.54	F_L	17

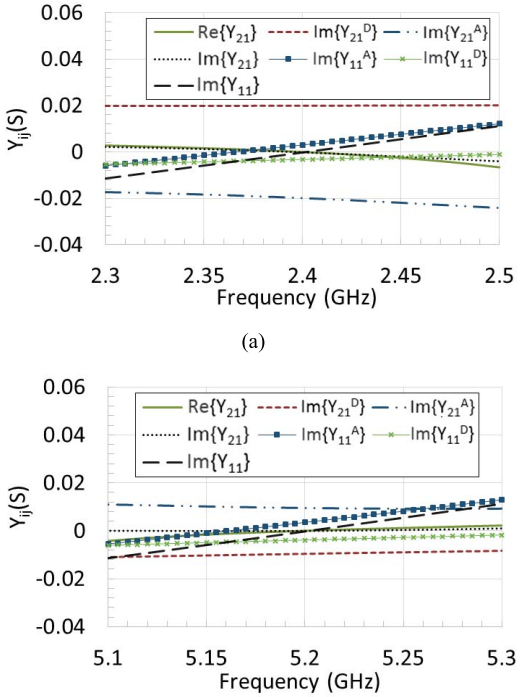

Fig. 15. Simulated total admittance Y_{ij} and imaginary part of Y_{ij}^A and Y_{ij}^D (a) in 2.4 GHz band and (b) 5.2 GHz band.

According to the simulated antenna parameters, the required parameter values are as follows: $\theta_1 = 83°$, $\theta_2 = 198°$, $Y_{21l}^A = -0.02$ S and $Y_{11l}^A = 0.003$ S at 2.4 GHz and $Y_{21h}^A = 0.0096$ S and $Y_{11h}^A = 0.0035$ at 5.2 GHz. Based on the design formulas discussed in Section II, the designed values are as follows: $\theta_{\alpha 0} = 72°$, $Z_\alpha = 36.3\ \Omega$, $\theta_{\beta 0} = 75.95°$, and $Z_\beta = 118\ \Omega$ for the first two phase-shifting T-stub; $\theta_{\alpha 0} = 73.2°$, $Z_\alpha = 39.8\ \Omega$, $\theta_{\beta 0} = 109.56°$, and $Z_\beta = 30.2\ \Omega$ for the third decoupling T-stub. It can be observed from Fig. 15 that having shunt connected the decoupling T-stub, the real part and the imaginary part of the total Y_{21} both become zero at the two frequencies. For the matching condition, a small imaginary part of the decoupling T-stub is designed to cancel out that of the antennas after adding the phase-shifting T-stub. In EM design, microstrip line is designed based on these derived transmission line characteristic impedances

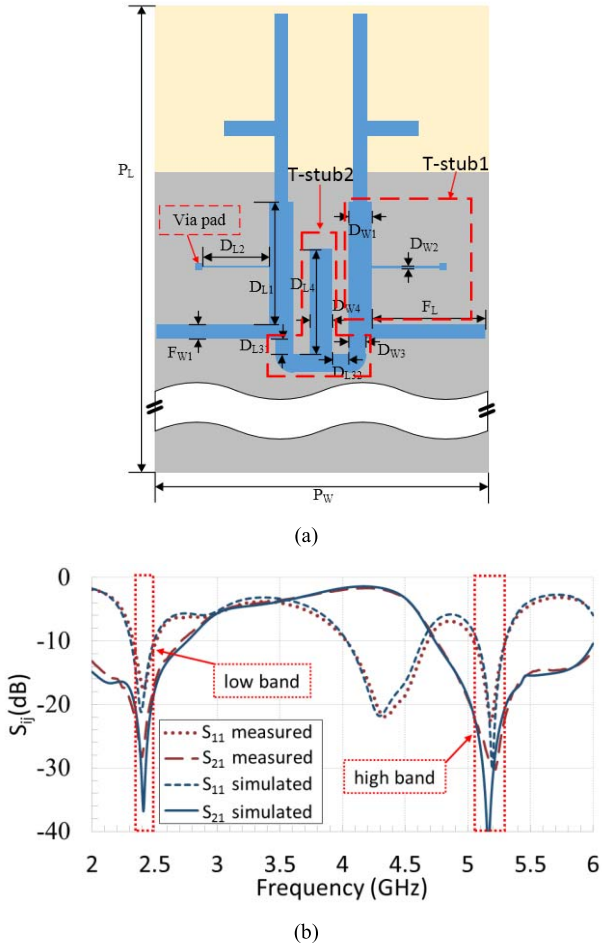

(a) (b)

Fig. 16. (a) Layout of two dual-band decoupled monopole antennas. (b) Simulated and measured S-parameters of the decoupled antennas.

and electrical lengths. Taking into consideration the via pads effect, fringe effect, and coupling between microstrip lines, a fine-tuning process is done in EM design. The layout of the decoupled dual-band monopole antennas is shown in Fig. 16(a) and the corresponding dimensions are given in Table III. The dotted rectangular boxes shown in Fig. 16(a) denote the decoupling circuit: T-stub 1 denotes the phase-shifting part while T-stub 2 denotes the decoupling part.

As shown in Fig. 16(b), the measured S-parameters agree well with the simulated results. The isolation between the two antennas is improved from about 5 dB to better than 18 dB in the low band (2.35 to 2.5 GHz) and 13 to 22 dB in the high band (5.05 to 5.3 GHz) while the return losses of the decoupled antennas is better than 10 dB in the two bands. The prototype of the coupled and decoupled dual-band monopole antennas are presented in Fig. 17.

The measured total efficiencies for both the low and high bands are compared in Fig. 18. It shows that in the low band, the efficiency is improved from about 65% to 95% by employing the decoupling circuit while in the high band, the efficiency improvement is smaller because the coupling S_{21} in high frequency band is about -13.5 dB but in low frequency band is about -5 dB.

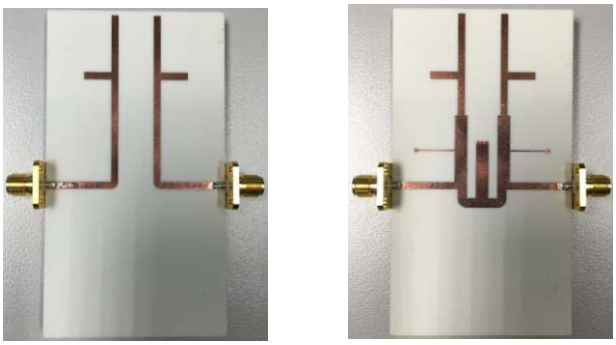

(a) (b)

Fig. 17. Prototypes of the coupled and decoupled dual-band monopole antennas. (a) Coupled antennas. (b) Decoupled antennas.

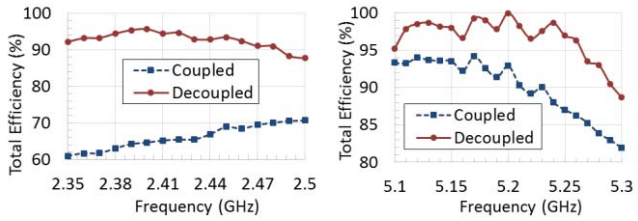

(a) (b)

Fig. 18. Measured total efficiency for coupled and decoupled monopole antennas (a) in 2.4 GHz band and (b) 5.2 GHz band.

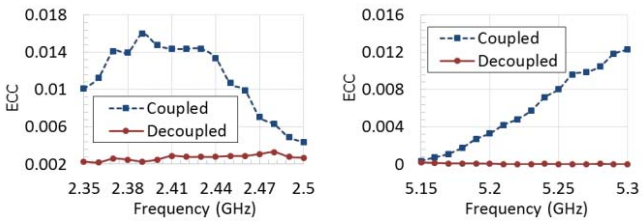

(a) (b)

Fig. 19. Measured total efficiency for coupled and decoupled antennas (a) in 2.4 GHz band and (b) 5.2 GHz band.

It is known that envelope correlation coefficients (ECC) is an important figure of merit for MIMO antennas. A lower ECC reflects a low correlation of two antennas. The ECC for the coupled and decoupled monopole antennas can be calculated according to the method introduced in [25], using the measured far-field radiation patterns. As shown in Fig. 19, a significant improvement for ECC is achieved using this decoupling network.

C. Discussion

The collateral effects should be discussed in this part. In the dual-band monopole example, the matching bandwidth of the low band after using this decoupling network becomes narrower compared with the coupled one. This phenomenon can be found in many previous works with strong coupling between the coupled antennas, such as about -4 dB in [7], -3 dB in [9], -4 dB at low band in [19]. In fact, the decoupled case in low band has a relatively wide bandwidth of 150 MHz

with 10 dB return loss and 18 dB isolation. In the first example, the matching bandwidths of both the low and high bands after using this decoupling network become wider compared with the coupled one. This verifies that the decoupling network will not directly increase or reduce the matching bandwidth of the antennas. This is understandable because the decoupling network is derived based on the two center frequencies so that it will not guarantee to increase or reduce the matching bandwidth of the antennas.

Another phenomenon is that the return loss of some frequencies between the two bands is less than 10 dB. In practical communication systems, there is a filter between transmitter/receiver and power amplifier to guarantee the signal of undesired frequency band does not flow into the system. For example, to reduce the interference from LTE band 40 (2.3–2.4 GHz), there is a bandpass filter after the WIFI (IEEE 802.11b, 2.4–2.484 GHz) antenna. Similar to reducing the interference from WIFI antenna, there is a bandpass filter after the LTE antenna.

IV. Conclusion

The T-stub circuit is investigated as a decoupling circuit of two coupled dual-band antennas in this paper. The decoupling circuit can concurrently perform the decoupling and matching in dual frequency bands independently. An analytical design formula for the T-stub of arbitrary dual-band phase shifting and impedance requirements is derived. The applicable solution regions of the proposed decoupling circuit that can meet the requirements for a large class of practical applications are also provided. Two decoupling examples incorporating two coupled dual-band inverted-F antennas and two coupled dual-band monopole antennas are provided to verify the proposed decoupling technique. Although the original coupled antennas are assumed to be well matched, the proposed decoupling circuit also works for those coupled antennas in poor matching conditions. Moreover, the proposed decoupling circuit is not limited to symmetric coupled antennas. The measured radiation performance demonstrates that the proposed decoupling technique can significantly improve the radiation efficiency as well as data throughput of a two-element dual-band MIMO system.

References

[1] M. A. Jensen and J. W. Wallace, "A review of antennas and propagation for MIMO wireless communications," *IEEE Trans. Antennas Propag.*, vol. 52, no. 11, pp. 2810–2824, Nov. 2004.

[2] C. Craeye and D. González-Ovejero, "A review on array mutual coupling analysis," *Radio Sci.*, vol. 46, no. 2, pp. 1–25, Apr. 2011, doi: 10.1029/2010RS004518.

[3] S. Hong *et al.*, "Applications of self-interference cancellation in 5G and beyond," *IEEE Commun. Mag.*, vol. 52, no. 2, pp. 114–121, Feb. 2014.

[4] J. Andersen and H. Rasmussen, "Decoupling and descattering networks for antennas," *IEEE Trans. Antennas Propag.*, vol. 24, no. 6, pp. 841–846, Nov. 1976.

[5] L. Yang, M. Fan, F. Chen, J. She, and Z. Feng, "A novel compact electromagnetic-bandgap (EBG) structure and its applications for microwave circuits," *IEEE Trans. Microw. Theory Techn.*, vol. 53, no. 1, pp. 183–190, Jan. 2005.

[6] A. Diallo, C. Luxey, P. Le Thuc, R. Staraj, and G. Kossiavas, "Study and reduction of the mutual coupling between two mobile phone PIFAs operating in the DCS1800 and UMTS bands," *IEEE Trans. Antennas Propag.*, vol. 54, no. 11, pp. 3063–3073, Nov. 2006.

[7] J. C. Coetzee and Y. Yu, "Port decoupling for small arrays by means of an eigenmode feed network," *IEEE Trans. Antennas Propag.*, vol. 56, no. 6, pp. 1587–1593, Jun. 2008.

[8] L. K. Yeung and Y. E. Wang, "Mode-based beamforming arrays for miniaturized platforms," *IEEE Trans. Microw. Theory Techn.*, vol. 57, no. 1, pp. 45–52, Jan. 2009.

[9] S.-C. Chang, Y.-S. Wang, and S.-J. Chung, "A decoupling technique for increasing the port isolation between two strongly coupled antennas," *IEEE Trans. Antennas Propag.*, vol. 56, no. 12, pp. 3650–3658, Dec. 2008.

[10] L. Zhao, K.-W. Qian, and K.-L. Wu, "A cascaded coupled resonator decoupling network for mitigating interference between two radios in adjacent frequency bands," *IEEE Trans. Microw. Theory Techn.*, vol. 62, no. 11, pp. 2680–2688, Nov. 2014.

[11] K. Qian, L. Zhao, and K.-L. Wu, "An LTCC coupled resonator decoupling network for two antennas," *IEEE Trans. Microw. Theory Techn.*, vol. 63, no. 10, pp. 3199–3207, Oct. 2015.

[12] M. S. Sharawi, A. B. Numan, M. U. Khan, and D. N. Aloi, "A dual-element dual-band MIMO antenna system with enhanced isolation for mobile terminals," *IEEE Antennas Wireless Propag. Lett.*, vol. 11, pp. 1006–1009, 2012.

[13] Y. Ding, Z. Du, K. Gong, and Z. Feng, "A novel dual-band printed diversity antenna for mobile terminals," *IEEE Trans. Antennas Propag.*, vol. 55, no. 7, pp. 2088–2096, Jul. 2007.

[14] X. Ling and R. Li, "A novel dual-band MIMO antenna array with low mutual coupling for portable wireless devices," *IEEE Antennas Wireless Propag. Lett.*, vol. 10, no. 1, pp. 1039–1042, Sep. 2011.

[15] I. Dioum, A. Diallo, S. M. Farssi, and C. Luxey, "A novel compact dual-band LTE antenna-system for MIMO operation," *IEEE Trans. Antennas Propag.*, vol. 62, no. 4, pp. 2291–2296, Apr. 2014.

[16] S. Yan, P. J. Soh, and G. A. E. Vandenbosch, "Dual-band textile MIMO antenna based on substrate-integrated waveguide (SIW) technology," *IEEE Trans. Antennas Propag.*, vol. 63, no. 11, pp. 4640–4647, Nov. 2015.

[17] X. Tang, K. Mouthaan, and J. C. Coetzee, "Dual-band decoupling and matching network design for very closely spaced antennas," in *Proc. 42nd Eur. Microw. Conf.*, Oct. 2012, pp. 49–52.

[18] P.-L. Chi, C.-J. Lee, and T. Itoh, "A compact dual-mand metamaterial-based rat-race coupler for a MIMO system application," in *IEEE MTT-S Int. Microw. Symp. Dig.*, Jun. 2008, pp. 667–670.

[19] K. C. Lin, C. H. Wu, C. H. Lai, and T. G. Ma, "Novel dual-band decoupling network for two-element closely spaced array using synthesized microstrip lines," *IEEE Trans. Antennas Propag.*, vol. 60, no. 11, pp. 5118–5128, Nov. 2012.

[20] L. Y. Zhao and K.-L. Wu, "A dual-band coupled resonator decoupling network for two coupled antennas," *IEEE Trans. Antennas Propag.*, vol. 63, no. 7, pp. 2843–2850, Jul. 2015.

[21] H. Zhang and K. J. Chen, "A stub tapped branch-line coupler for dual-band operations," *IEEE Microw. Wireless Compon. Lett.*, vol. 17, no. 2, pp. 106–108, Feb. 2007.

[22] P. Saad, P. Colantonio, L. Piazzon, F. Giannini, K. Andersson, and C. Fager, "Design of a concurrent dual-band 1.8–2.4-GHz GaN HEMT Doherty power amplifier," *IEEE Trans. Microw. Theory Techn.*, vol. 60, no. 6, pp. 1840–1849, Jun. 2012.

[23] K. Rawat and F. M. Ghannouchi, "Design methodology for dual-band Doherty power amplifier with performance enhancement using dual-band offset lines," *IEEE Trans. Ind. Electron.*, vol. 59, no. 12, pp. 4831–4842, Dec. 2012.

[24] *SystemVue Electronic System-Level (ESL) Design Software*, Agilent Technol., Santa Clara, CA, USA, 2013.

[25] R. G. Vaughan and J. B. Andersen, "Antenna diversity in mobile communications," *IEEE Trans. Veh. Technol.*, vol. 36, no. 4, pp. 147–172, Nov. 1987.

Jiangwei Sui received the B.S. degree in electronic engineering from the University of Science and Technology of China, Hefei, China, in 2014. He is currently pursuing the Ph.D. degree at the Chinese University of Hong Kong, Hong Kong.

His current research interests include antenna design and applications for mobile communication systems, passive RF and microwave components, and devices and systems.

Ke-Li Wu (M'90–SM'96–F'11) received the B.S. and M.Eng. degrees from the Nanjing University of Science and Technology, Nanjing, China, in 1982 and 1985, respectively, and the Ph.D. degree from Laval University, Québec, QC, Canada, in 1989.

From 1989 to 1993, he was a Research Engineer and a Group Manager with the Communications Research Laboratory, McMaster University, Hamilton, ON, Canada. In 1993, he joined the Corporate Research and Development Division, COM DEV International, where he was a Principal Member of Technical Staff. Since 1999, he has been with the Chinese University of Hong Kong, Hong Kong, where he is currently a Professor and the Director of the Radiofrequency Radiation Research Laboratory. He has authored and co-authored numerous publications in the areas of electromagnetic (EM) modeling and microwave passive components, microwave filter, and antenna engineering. His current research interests include partial-element equivalent circuits and physically derived micromodeling circuits for high-speed circuits, RF and microwave passive circuits and systems, synthesis theory and robot automatic tuning of microwave filters, decoupling techniques for multiple antennas in both wireless terminals, and massive multiple-input multiple output array antennas.

Dr. Wu is a member of the IEEE MTT-8 Subcommittee (Filters and Passive Components) and also serves as a TPC Member of many prestigious international conferences including the International Microwave Symposium. He was a recipient of the 1998 COM DEV Achievement Award for the development of exact EM design software of microwave filters and multiplexers and the Asia–Pacific Microwave Conference Prize in 2008 and 2012, respectively. He was an Associate Editor of the IEEE TRANSACTIONS ON MICROWAVE THEORY AND TECHNIQUES from 2006 to 2009.